Rare Met. (2018) 37(3):237–242
https://doi.org/10.1007/s12598-017-0887-8

RARE METALS
www.editorialmanager.com/rmet

Achievement of high performance of sintered R–Fe–B magnets based on misch metal doped with PrNd nanoparticles

Qiang Ma, Jian-Teng Zhu, Xue-Feng Zhang*, Zeng-Ru Zhao, Yan-Li Liu, Gao-Feng Wang, Yong-Feng Li, Zhu-Bai Li

Received: 18 May 2016 / Revised: 22 June 2016 / Accepted: 4 February 2017 / Published online: 6 April 2017

Abstract The magnetic properties and microstructure of sintered R–Fe–B (R, rare earth) magnets with nominal composition of $((PrNd)_{1-x}MM_x)_{30}Fe_{bal}B_1$ ($x = 0$, 0.1, 0.2, 0.3, 0.4, 0.5 and 0.7; MM, misch metal) prepared using dual-alloy method were investigated. For $x = 0.3$, the maximum energy product ($(BH)_{max}$) of the sintered magnet is higher than 318.4 $kJ{\cdot}m^{-3}$, but intrinsic coercivity (H_{cj}) is lower than 351.8 $kA{\cdot}m^{-1}$. The La and Ce contents are obviously different in some matrix-phase grains, which proves that the multi-hard magnetic phases (La, Ce-rich and La, Ce-lean) exist in the magnets. The coercivity is improved by the method of doping PrNd nanoparticles without sacrificing other magnetic properties. An enhancement in coercivity from 517.2 to 872.9 $kA{\cdot}m^{-1}$ is achieved by doping 5 wt% PrNd nanoparticles. Meanwhile, it could exhibit better magnetic properties (remanence $B_r = 1.332$ T, intrinsic coercivity $H_{cj} = 872.9$ $kA{\cdot}m^{-1}$, maximum energy product $(BH)_{max} = 318.6$ $kJ{\cdot}m^{-3}$) and make the distribution of the intergranular phase become more homogeneous.

Keywords Permanent magnetic materials; Nanoparticles; Misch metal; Dual-alloy; Coercivity

Q. Ma, J.-T. Zhu, X.-F. Zhang*, Z.-R. Zhao, Y.-L. Liu, G.-F. Wang, Y.-F. Li, Z.-B. Li
Key Laboratory of Integrated Expoitation of Bayan Obo Multi-Metal Resources, Inner Mongolia University of Science and Technology, Baotou 014010, China
e-mail: xuefeng367@163.com

Q. Ma, J.-T. Zhu, X.-F. Zhang, Z.-R. Zhao, Y.-L. Liu, Y.-F. Li
College of Science, Inner Mongolia University of Science and Technology, Baotou 014010, China

1 Introduction

Since discovery of excellent magnets Nd–Fe–B in 1983, they have become the most widely used type of rare earth permanent magnets [1–3]. Rare earth permanent magnetic materials play important roles in economics and lives. However, it consumes mainly low-abundant rare earth elements to produce traditional rare earth permanent magnets, leading to the extreme unbalance in the utilization of resources. The consumption of Nd and Pr increases significantly due to the increasing production of Nd–Fe–B permanent magnets in the world. Moreover, the rare earth mineral is paragenic. Pr and Nd only account for 22 wt% of light rare earth metals, and La (≥25 wt%) and Ce (≥47 wt%) are the most abundant and the cheapest in the mineral. Developing high-abundant rare earth permanent magnets is necessary not only for reducing cost, but also for efficient utilization of the resources. Recently, the substitution of Pr–Nd by Ce [4–8] or misch metal (MM) alloys has attracted renewed attention [9–12]. However, the magnetic properties of magnet based on misch metal were found to be low [13–16]. The magnitude of coercivity does not meet the application of medium- and high-grade products.

In this work, it was taken advantage of double main phase alloy method to manufacture high-performance R–Fe–B permanent magnets with low production cost. The commonly associated rare earth permanent magnets were prepared using misch metal to save the Pr, Nd resources. This method avoids unnecessary separation process of rare earth elements, which utilizes the resources efficiently and protects the environment. Moreover, the method of doping PrNd nanoparticles was introduced in an attempt to improve the coercivity of sinter magnets containing MM [17–19]. Magnetic properties and magnetic domain of MM

magnet with MM accounting for 30% of total rare earth elements were surveyed.

2 Experimental

The raw material MM is one of the typical misch metals from Bayan Obo mine in Baotou, China. It consists of 28.63 wt% La, 50.13 wt% Ce, 4.81 wt% Pr, 16.38 wt% Nd and other inevitable impurities. According to the dual-alloy method, two alloys with nominal compositions of $(Pr,Nd)_{30}Fe_{bal}B_1$ and $((PrNd)_{0.3}MM_{0.7})_{30}Fe_{bal}B_1$ were prepared by strip casting (SC) technique. The two varieties cast strips independently performed hydrogen decrepitation and jet-milling to obtain powders with an average particle size of 3–5 μm. And then the two powders were mixed together according to the nominal composition of $((PrNd)_{1-x}MM_x)_{30}Fe_{bal}B_1$ (wt%, $x = 0$, 0.1, 0.2, 0.3, 0.4, 0.5 and 0.7), respectively. The powders were compacted after aligning under a constant magnetic field of 1.8 T and compacting under a pressure of 30 MPa. Then the green compacts were sintered at 1010–1060 °C for 2 h under a vacuum of 4.5×10^{-3} Pa. Subsequently, the sintered magnets were annealed at 900 °C for 110 min and then post-annealed at 600 °C for 120 min. In order to improve coercivity, the powders with nominal composition of $((PrNd)_{0.7}MM_{0.3})_{30}Fe_{bal}B_1$ and the PrNd (a composition of $Pr_{25.5}Nd_{74.5}$ (wt%)) nanoparticles were homogeneously mixed. The PrNd nanoparticles powders were prepared by the inert gas condensing method using direct current (DC) arc plasma metal nanometer powder preparation equipment (ZJ-NM-KY). The magnets were prepared by blended powder. The density of the magnets was measured by water immersion method at room temperature. The magnetic properties of the samples were measured using an NIM-2000 magnetic measuring device. The heat flow measurements were taken by a differential scanning calorimeter (DSC, STA449C-2). The phases of the magnets were characterized using X-ray diffractometer (XRD, PANalytical X'pert Powder) with Co Kα radiation. Microstructural investigations of the samples were carried out using scanning electron microscope (SEM, FEI Nova Nano 200) equipped with energy-dispersive spectroscope (EDS) and transmission electron microscope (TEM, JEM-2100). Domain structure was observed using a BH-786IP-PK high-field Kerr microscopy.

3 Results and discussion

The magnetic properties of $((PrNd)_{1-x}MM_x)_{30}Fe_{bal}B_1$ ($x = 0$, 0.1, 0.2, 0.3, 0.4, 0.5 and 0.7) magnets are shown in Fig. 1. It can be noticed from Fig. 1 that remanence (B_r), maximum energy product ($(BH)_{max}$), intrinsic coercivity (H_{cj}) and density (ρ) gradually decrease with the increase of MM content accounting for the total rare earth amount, referred to as MM/R. It is due to the fact that the intrinsic magnetic properties of $La_2Fe_{14}B$ and $Ce_2Fe_{14}B$ are far inferior to those of $Nd_2Fe_{14}B$. For $La_2Fe_{14}B$ and $Ce_2Fe_{14}B$, the saturation polarizations ($4\pi M_s$) are 1.38 and 1.17 T, and the magnetocrystalline anisotropy fields (H_A) are 2000 and 3600 kA·m^{-1} [2], respectively. For the substitution of MM for Pr and Nd, the $R_2Fe_{14}B$ (R = La, Ce, Pr, Nd) phase forms, which decreases the magnetic polarization and anisotropy field in the magnet. It can be clearly seen that H_{cj} decreases with the increase of MM/R. H_{cj} declines rapidly to the value of 668.4 kA·m^{-1} for MM/R ≤ 20% and then slowly for MM/R ≥ 20%. For MM/R = 20%, the magnetic properties reach a preferable level of $B_r = 1.326$ T, $H_{cj} = 666.0$ kA·m^{-1} and $(BH)_{max} = 330.2$ kJ·m^{-3}. In addition, H_{cj} declines significantly for MM/R = 30%.

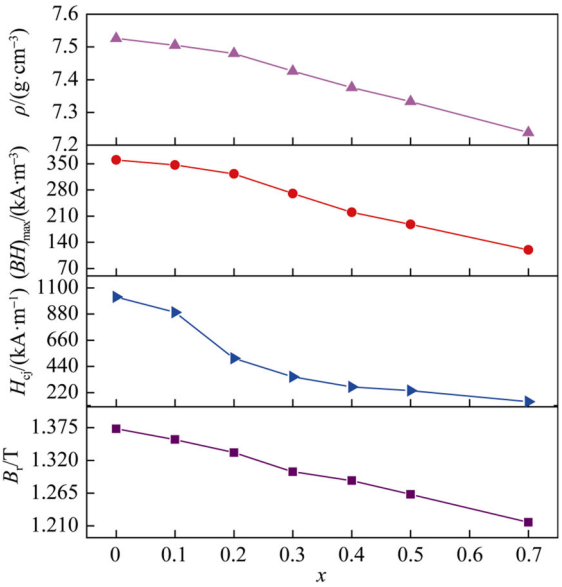

Fig. 1 Magnetic properties of $((PrNd)_{1-x}MM_x)_{30}Fe_{bal}B_1$ magnets at room temperature

XRD patterns of $((PrNd)_{1-x}MM_x)_{30}Fe_{bal}B_1$ ($x = 0$, 0.1, 0.2, 0.3, 0.4, 0.5 and 0.7) magnets are shown in Fig. 2. It can be seen from Fig. 2 that the magnets consist mainly of $R_2Fe_{14}B$ phase (R = La, Ce, Pr, Nd). A small amount of $CeFe_2$ is observed ($2\theta \approx 41°$ and 47°) in the magnet with low coercivity. $CeFe_2$ is not only stable in equilibrium R–Fe binary alloy system, but also paramagnetic at room temperature [20]. In addition, the R-rich phases are also observed ($2\theta \approx 35°$) in the magnet. It can be noticed that the intensity of diffraction peak of R-rich phase becomes disorganized with the increase of MM/R. Therefore, the existence of impurity phase may harm the coercivity among the boundaries of the grains.

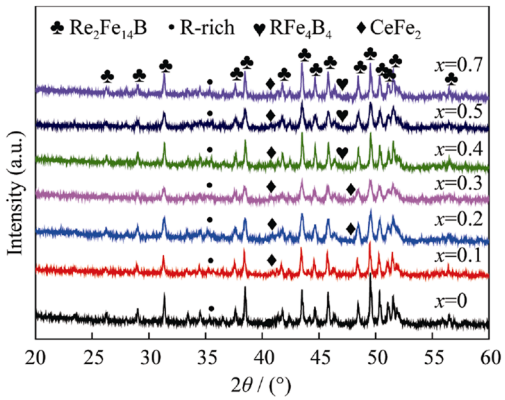

Fig. 2 XRD patterns of $((PrNd)_{1-x}MM_x)_{30}Fe_{bal}B_1$ magnet samples after sintering and annealing

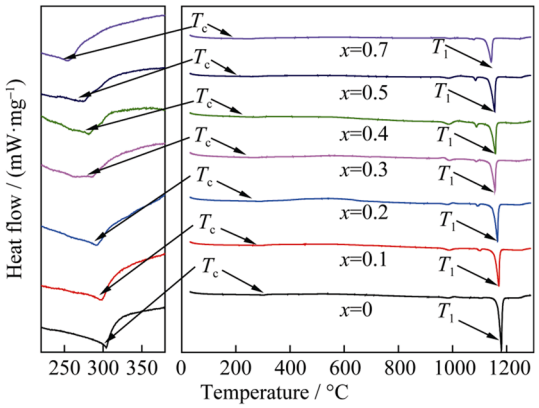

Fig. 3 DSC curves of $((PrNd)_{1-x}MM_x)_{30}Fe_{bal}B_1$ magnets with different MM contents

Figure 3 displays DSC curves of $((PrNd)_{1-x}MM_x)_{30}Fe_{bal}B_1$ ($x = 0$, 0.1, 0.2, 0.3, 0.4, 0.5 and 0.7). Endothermic peaks at T_C in Fig. 3 refer to the Curie temperatures of the magnets, at which the main phase changes from ferromagnetic to paramagnetic. It can be noticed from Fig. 3 that the Curie temperatures of the $((PrNd)_{1-x}MM_x)_{30}Fe_{bal}B_1$ magnets decrease with the increase of MM contents. The Curie temperatures of $R_2Fe_{14}B$ phase are 304.0, 296.7, 288.6, 281.0, 280.1, 255.0 and 253.0 °C for $x = 0$, 0.1, 0.2, 0.3, 0.4, 0.5 and 0.7, respectively. Endothermic peaks at T_1 in Fig. 3 refer to the melting temperatures of the $R_2Fe_{14}B$ phases, at which the main phase changes from solid to liquid phase. It can be noticed from Fig. 3 that the melting temperatures of $R_2Fe_{14}B$ phase are 1180.7, 1169.8, 1167.7, 1158.3, 1157.9, 1155.6 and 1142.7 °C for $x = 0$, 0.1, 0.2, 0.3, 0.4, 0.5 and 0.7, respectively. Above results are due to that the Curie temperatures of $Ce_2Fe_{14}B$ and $La_2Fe_{14}B$ are lower than that of Nd_2Fe14B [21]. In addition, some La and Ce enter into $R_2Fe_{14}B$ phase, resulting in the decrease of the melting temperature of $R_2Fe_{14}B$ phase [21, 22]. This indicates that adding MM can reduce the Curie temperatures and the melting temperatures of $R_2Fe_{14}B$ phases. So the magnets can be sintered and annealed at lower temperature.

SEM images of magnets are shown in Fig. 4, and EDS analysis data are listed in Table 1 for different regions of the sample with nominal composition of $((PrNd)_{0.8}MM_{0.2})_{30}Fe_{bal}B_1$ and $((PrNd)_{0.3}MM_{0.7})_{30}Fe_{bal}B_1$. The gray areas correspond to $R_2Fe_{14}B$ phase, and the white areas correspond to intergranular phase. It can be seen in Fig. 4 that LaCe-rich (marked as C, E) and LaCe-lean (marked as A, B, F, G, H) matrix grains exist in the magnets. Many triple-junction phases of R-rich phase with more La and Ce elements are observed in Fig. 4, as listed in Table 1. La and Ce contents in Regions 3 and 4 are more than those in Regions 1 and 5 in Fig. 4, respectively. Agglomeration occurs easily in LaCe-rich intergranular phase. The R-rich phase exists among the boundaries of the grains, which weakens the coupling between the hard phase grains [23–26]. The decrease of partial R-rich phase results in the abnormal triple-junction R-rich phases. Besides, since the coupling between the hard phase grains reinforces which is related to the abnormal triple-junction R-rich phases, the coercivity gradually decreases with the increase of MM contents. The agglomeration of the R-rich phase is observed in sintering R–Fe–B permanent magnets containing MM, which leads to such a low magnetic properties in the magnets.

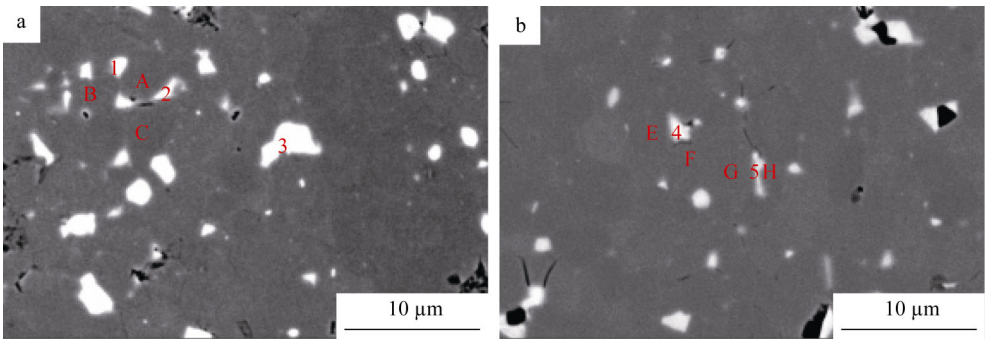

Fig. 4 SEM back-scattered images of $((PrNd)_{1-x}MM_x)_{30}Fe_{bal}B_1$ magnets with **a** $x = 0.2$ and **b** $x = 0.7$

Table 1 Compositions of regions in Fig. 4a, b determined by EDS (wt%)

Regions	La	Ce	Pr	Nd	Fe	O
A	1.57	1.66	5.83	22.66	67.59	0.69
B	1.59	1.10	5.08	23.00	68.61	0.61
C	4.88	10.21	3.11	12.75	68.45	0.59
1	8.08	5.98	16.93	59.49	6.04	3.49
2	10.78	9.86	14.86	38.32	25.54	0.60
3	15.21	6.17	16.63	53.44	1.97	6.58
E	6.25	10.51	2.46	11.39	68.63	0.76
F	3.81	8.44	3.70	12.02	71.28	0.75
G	4.61	8.72	3.52	14.59	67.68	0.88
H	4.59	8.75	3.42	13.15	69.46	0.63
4	43.87	22.00	7.59	16.22	9.29	1.03
5	33.57	14.41	9.10	29.23	8.38	5.32

SEM image of $((PrNd)_{1-x}MM_x)_{30}Fe_{bal}B_1$ powders and TEM image of PrNd nanoparticles are shown in Fig. 5. The size of $((PrNd)_{1-x}MM_x)_{30}Fe_{bal}B_1$ powders and PrNd nanoparticles are about 3–5 μm and 50–80 nm, respectively. In order to improve coercivity, PrNd nanoparticles were added to the $((PrNd)_{0.7}MM_{0.3})_{30}Fe_{bal}B_1$ magnet by dual-alloy method. Table 2 shows the rare earth contents of the magnets with MM/R = 20% (S_1) and MM/R = 30% with 5 wt% PrNd nanoparticles (S_2). The total rare earth content ($\sum RE/R_m$) increases from 30 wt% in S_1 to 33.4 wt% in S_2, which may lead to the enhancement of the coercivity. Nd(Pr)/R_m increases from 24 wt% in S_1 to 24.8 wt% in S_2 and MM/R_m increases from 6 wt% in S_1 to 8.6 wt% in S_2. Consequently, the production cost is reduced by the increase of MM content. Demagnetization curves of the magnets as a function of doping content of PrNd nanoparticles are shown in Fig. 6. The coercivity improves with the increase of PrNd nanoparticles content. The magnetic properties (B_r = 1.332 T, H_{cj} = 872.9 kA·m^{-1}, $(BH)_{max}$ = 318.6 kJ·m^{-3}) of the magnet used dual-alloy method with 5 wt% PrNd nanoparticles are better than

Table 2 Rare earth content of MM/R = 20% (S_1) and MM/R = 30% with 5 wt% PrNd nanoparticles (S_2) magnets (wt%)

Samples	Pr(Nd)/R_m	MM/R_m	$\sum$RE/R_m	MM/R
S_1	24.0	6.0	30.0	20.0
S_2	24.8	8.6	33.4	25.7

R_m, total mass of magnets

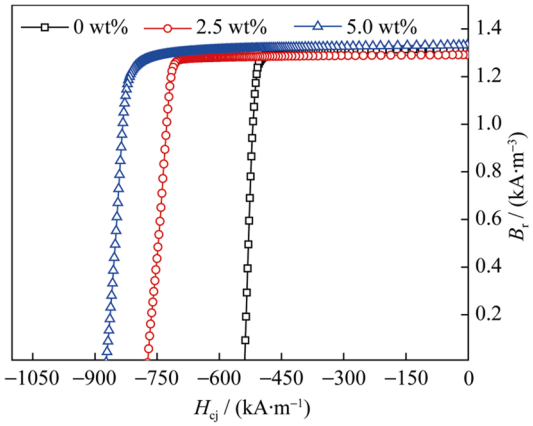

Fig. 6 Demagnetization curves of sintered $((PrNd)_{0.7}MM_{0.3})_{30}Fe_{bal}B_1$ magnets with different doping contents of PrNd nanoparticles

those of the magnet without PrNd nanoparticles doping. The MM/R reduces to 25.7% for the magnet with 5 wt% PrNd nanoparticles, but the magnetic properties exceed those of the magnet with MM/R = 20%.

To study the reason for coercivity change, the magnetic domain structures of the magnet with and without PrNd nanoparticles doping are shown in Fig. 7. The magnets were cut into a dimension of 3 mm × 8 mm × 5 mm with the easy axis along the long direction of the sample. The surfaces of the samples were polished for clearly revealing domain configuration. It can be seen from Fig. 7 that bright and dark domains are observed in same grain. Many continuous domains are found in the magnet without PrNd

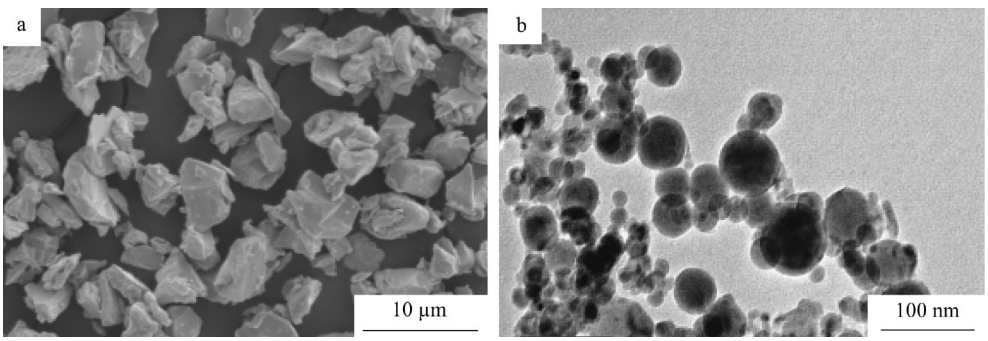

Fig. 5 SEM image of $((PrNd)_{0.7}MM_{0.3})_{30}Fe_{bal}B_1$ **a** and TEM image of PrNd nanoparticles **b**

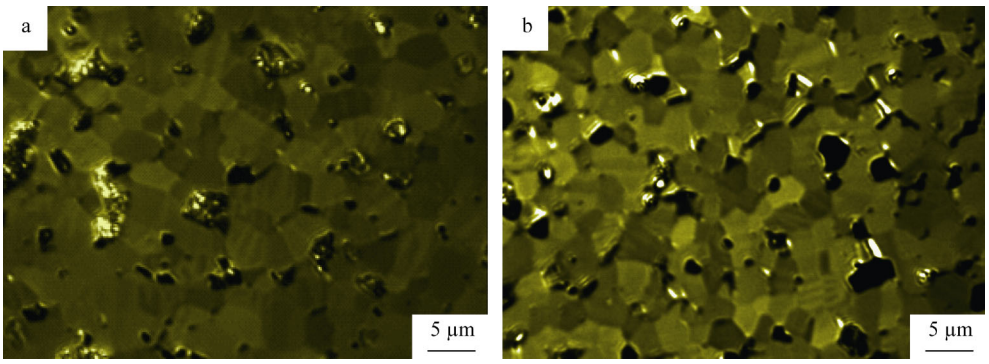

Fig. 7 Domain patterns of $((PrNd)_{0.3}MM_{0.7})_{30}Fe_{bal}B_1$ magnet **a** without and **b** with 5 wt% PrNd nanoparticles doping

nanoparticles through the grain boundary in Fig. 7a. For the magnet with 5wt% PrNd nanoparticles doping, continuous domains decrease with the increase of PrNd nanoparticles content in the magnet in Fig. 7b. Magnets with homogenous distribution of R-rich phase normally exhibit excellent magnetic properties [27–30]. Improvement of the coercivity may be caused by the fact that the Re-rich phase becomes homogeneous in the magnet with the addition of PrNd nanopowders. It not only favors the isolation of adjacent hard magnetic grains, but also attaches to the surface of the $Nd_2Fe_{14}B$ grains by taking the form of particle phase.

4 Conclusion

The magnetic properties of R–Fe–B prepared with different ratios of MM–Fe–B and Nd–Fe–B were systematically investigated. The results show that the magnetic properties decrease gradually with the increase of MM content, but they still have potential to manufacture permanent magnets. H_{cj} gradually decreases with the increase of MM contents because of the agglomeration of R-rich phase. The coercivity enhances with PrNd nanoparticles content increasing, whereas both the remanence and the maximum energy product reach the maximum values with 5 wt% PrNd doping. The maximum energy product is 318.6 $kJ{\cdot}m^{-3}$ and coercivity is 872.9 $kA{\cdot}m^{-1}$ for MM/R = 25.7%. Domain investigation shows that the continuous domains are reduced by PrNd nanoparticle doping. Therefore, it is concluded that PrNd nanoparticle doping is an efficient method to improve coercivity in R–Fe–B magnets containing MM.

Acknowledgements This study was financially supported by the National Key Research and Development Program of China (No. 2016YFB0700903), the National Natural Science Foundation of China (No. 51571126), the Inner Mongolia Innovative Research Team (No. 3400102), the Innovative Science and Technology Project of Inner Mongolia (No. 4140300502), the Science and Technology Project of Baotou (Nos. 2012R1006 and 2015C2006-13) and the Science and Technology Innovation Project of University (No. 2014QDL003).

References

[1] Sagawa M, Fujimura S, Togawa N, Yamamoto H, Matsuura Y. New material for permanent magnets on a base of Nd and Fe. J Appl Phys. 1984;55(6):2083.
[2] Herbst JF. $R_2Fe_{14}B$ materials: intrinsic properties and technological aspects. Rev Mod Phys. 1991;63:819.
[3] Li ZB, Shen BG, Zhang M, Zhang Y, Hu FX, Sun JR. Irreversible magnetization and self-interaction investigated by thermal activation in $Pr_2Fe_{14}B$ magnets. Appl Phys Lett. 2015;106(4):042403.
[4] Zhu MG, Li W, Wang JD, Zheng LY, Li YF, Zhang K, Feng HB, Liu T. Influence of Ce content on the rectangularity of demagnetization curves and magnetic properties of R-Fe-B magnets. IEEE Trans Magn. 2014;50(1):1000104.
[5] Huang SL, Feng HB, Zhu MG, Li AH, Zhang Y, Li W. Preparation of sintered $(Ce_{1-x}Nd_x)_{30}Fe_{bal}Cu_{0.1}B_1$ by blending powder method. J Iron Steel Res Int. 2015;22(7):598.
[6] Niu E, Chen ZA, Chen GA, Zhao YG, Zhang J, Rao XL, Hu BP, Wang ZX. Achievement of high coercivity in sintered R-Fe-B magnets based on misch-metal by dual alloy method. J Appl Phys. 2014;115(11):113912.
[7] Yan CJ, Guo S, Chen RJ, Lee D, Yan AR. Phase constitution and microstructure of Ce–Fe–B strip-casting alloy. Chin Phys B. 2014;23(10):107501.
[8] Zhang XF, Lan JT, Li ZB, Liu YL, Zhang LL, Li YF, Zhao Q. Abnormal variation of magnetic properties with Ce content in $(PrNdCe)_2Fe_{14}B$ sintered magnets prepared by dual alloy method. Chin Phys B. 2016;25(5):057502.
[9] Ko KY, Yoon S, Booth JG. Magnetic properties and microstructure of hot-pressed and die-upset mischmetal-FeB-(Al)permanent magnets. J Magn Magn Mater. 1997;176(2–3):313.
[10] Bulyk II, Panasyuk VV, Trostianchyn AM, Grygorenko GM, Pomarin YM, Taranova TG, Kostin VA, Putilov YG. Features of the HDDR process in R-Fe–B ferromagnetic alloys(R is a mixture of Nd, Pr, Ce, La, Dy and others). J Alloys Comp. 2004;370(1–2):261.
[11] Ko KY, Yoon S, Booth JG, Al-Kanani HJ, Cho SK. Magnetic properties and microstructures of mischmetal-FeB-(Al, Ti and Al–Co) permanent magnets. J Mater Sci. 2002;37(7):1421.
[12] Zhang M, Shen BG, Hu FX, Sun JR. Effect of Si substitution on structure and magnetic properties in mischmetal-Fe–B ribbons. IEEE Trans Magn. 2015;51(11):2103304.
[13] Tang W, Wu YQ, Dennis KW, Oster NT, Kramer MJ. Studies of microstructure and magnetic properties in sintered mixed rare

earth (MRE)-Fe–B magnets (MRE = Nd + La + Dy). J Appl Phys. 2011;109(07):07A704.
[14] Tang W, Wu YQ, Oster NT, Dennis KW, Kramer MJ. Improved energy product in grained aligned and sintered $MRE_2Fe_{14}B$ magnets (MRE = Y + Dy + Nd). J Appl Phys. 2010;107(9): 09A728.
[15] Skoug EJ, Meyer MS, Pinkerton FE, Tessema MM, Haddad D, Herbst JF. Crystal structure and magnetic properties of $Ce_2Fe_{14-x}Co_xB$ alloys. J Alloys Compd. 2013;574(10):552.
[16] Chang WC, Wang SH, Chang SJ, Chen Q. Magnetic and microstructure studies of boron-enriched $(Nd_{0.95}La_{0.05})_{11}Fe_{76.5-x}Co_xTi_2B_{10:5}$($x$ = 0–15) melt-spun ribbons. IEEE Trans Magn. 2000;36(5):3312.
[17] Liu WQ, Sun H, Yi XF, Liu XC, Zhang DT, Yue M, Zhang JX. Coercivity enhancement in Nd–Fe–B sintered permanent magnet by Dy nanoparticles doping. J Alloys Compd. 2010;501(1): 67.
[18] Liu WQ, Li C, Zakotnik M, Yue M, Zhang DT, Huang XL. Recycling of waste Nd–Fe–B sintered magnets by doping with dysprosium hydride nanoparticles. J Rare Earths. 2015;33(8):846.
[19] Zhang XF, Liu F, Liu YL, Ma Q, Li YF, Zhao Q, Gf Wang, Li ZB. Recycling of sintered Nd–Fe–B magnets doped with PrNd nanoparticles. J Magn. 2015;20(2):97.
[20] Herbst JF, Meyer MS, Pinkerton FE. Magnetic hardening of $Ce_2Fe_{14}B$. J Appl Phys. 2012;11(07):07A718.
[21] Deportes J, Givord D, Ziebeck KRA. Evidence of short range magnetic order at four times T_c in a metallic compound containing Fe: susceptibility and paramagnetic scattering in $CeFe_2$. J Appl Phys. 1981;52(3):2074.
[22] Liu XB, Altounian Z, Huang MD, Zhang QM, Liu JP. The partitioning of La and Y in Nd–Fe–B magnets: a first-principles study. J Alloys Compd. 2013;549(5):366.
[23] Ju JY, Tang X, Chen RJ, Wang JZ, Yin WZ, Li D, Yan AR. Fine-grained NdFeB magnets prepared by low temperature pre-sintering and subsequent hot pressing. Chin Phys B. 2015; 24(1):493.
[24] Deng Y, Zhao GP, Chen L, Zhang HW, Zhou XL. Reduced exchange coupling and hysteresis loops in two-phased magnetic nanosystem. J Magn Magn Mater. 2011;323(5):535.
[25] Zhao GP, Deng Y, Zhang HW, Cheng ZH, Ding J. Accurate calculation of the nucleation field and hysteresis loops in hard-soft multilayers. J Appl Phys. 2011;109(07):15.
[26] Yan CJ, Guo S, Chen RJ, Lee D, Yan AR. Effect of Ce on the magnetic properties and microstructure of sintered didymium-Fe–B magnets. IEEE Trans Magn. 2014;50(10):2102605.
[27] Sepehri-Amin H, Ohkubo T, Shima T, Hono K. Grain boundary and interface chemistry of an NdFeB-based sintered magnet. Acta Mater. 2012;60(3):819.
[28] Liu J, Sepehri-Amin H, Ohkubo T, Hioki K, Hattori A, Schrefl T, Hono K. Effect of Nd content on the microstructure and coercivity of hot-deformed Nd–Fe–B permanent magnets. Acta Mater. 2013;61(14):3365387.
[29] Zhao GP, Zhao MG, Lim HS, Feng YP, Ong CK. From nucleation to coercivity. Appl Phys Lett. 2005;87(16):162513.
[30] Li YF, Lai B, Zhu MG, Feng HB, Li W, Du A. Mechanism on control technology of grain boundary phase in sintered Nd-Fe-B magnets. Rare Met. 2015;39(11):988.